ELSEVIER

Materials Science and Engineering B 126 (2006) 112–119

MATERIALS SCIENCE & ENGINEERING B

www.elsevier.com/locate/mseb

Spin filtering effects in monocristalline Fe/MgO/Fe magnetic tunnel junctions

C. Tiusan*, J. Faure-Vincent, M. Sicot, M. Hehn, C. Bellouard, F. Montaigne, S. Andrieu, A. Schuhl

Laboratoire de Physique des Matériaux, UMR CNRS 7556, B.P. 239, 54506 Vandœuvre lès Nancy Cedex, France

Abstract

Single-crystal magnetic tunnel junctions employing bcc (1 0 0) Fe electrodes and MgO(1 0 0) insulating barrier are elaborated by molecular beam epitaxy. Two extreme regimes have been investigated. First, for extremely thin MgO thickness we show that the equilibrium tunnel transport in Fe/MgO/Fe systems leads to antiferromagnetic interactions, mediated by the tunneling of the minority spin interfacial resonance state. Second, for large MgO barrier thickness, the tunnel transport validates specific spin filtering effect in terms of symmetry of the electronic Bloch function and symmetry-dependent wave function attenuation in the single-crystal barrier. Within this framework, we present giant tunnel magnetoresistive effects at room temperature (125–150%). Moreover, we illustrate that the interfacial chemical and electronic structure plays a crucial role in the filtering. We show that the insertion of carbon impurities at the Fe/MgO interface changes radically the voltage response of the tunnel magnetoresistance. Moreover, we provide experimental evidence for the electronic interfacial resonance states contribution to the spin polarized tunnel transport.

Keywords: Spin electronics; Magnetic tunnel junctions; Epitaxial layers; Spin dependent tunneling; Tunnel magnetoresistance

1. Introduction

The discovery of a tunnel magnetoresistance (TMR) effect at room temperature in amorphous oxide barrier based magnetic tunnel junctions (MTJ) [1] paved the way to intense developments in this field area with many possible application prospects [2]. Recently, this subject has been boosted with the measure at room temperature of TMR values above 200% in MgO crystalline oxide based tunnel barriers [3–5], three times larger than in standard amorphous alumina barriers. These large TMR ratios are determined by the different tunneling mechanisms and symmetry-related decay rates of the Bloch waves for the majority and the minority spin channels.

Roughly, an emitter single-crystalline ferromagnetic (FM) electrode filters in terms of symmetry the electrons subsequently injected across the insulating (*I*) barrier. The filtering effect can be easily understood from Fig. 1, where we illustrate the bulk band structure of bcc Fe, along the $\Gamma - H$ direction, for the majority and minority spins. At the Fermi level for the majority electrons we have the following states: a Δ_1 (spd-like character state), a Δ_5 (pd) and a $\Delta_2^{'}$ (d). Due to the exchange splitting, there is no Δ_1 state for the minority spin. Therefore, one can immediately see that the Fe behaves as a half-metal system in terms of the Δ_1 symmetry. The tunnel transport probes: (i) the differences in spin injection (extraction) efficiency (directly related to the interfacial FM/I matching/coupling), and (ii) the differences in decay rates when tunneling across the barrier. The epitaxial growth of the MgO on Fe, via a rotation by 45° of the MgO lattice with respect to the Fe one, provides the symmetry conservation across the junction stack. One can demonstrate that the Δ_1 state has the smallest decay rate across the MgO, followed by the Δ_5, then the $\Delta_{2,2'}$.

Consequently [6,7], for large MgO thickness, in the asymptotic regime, in the parallel (*P*) configuration, the tunneling is found to be governed by the Δ_1 state. The conductance in the antiparallel (AP) configuration is very low, being only related to the $\Delta_{5,2'}$ state propagation, with a larger decay rate. In the AP configuration, an injected Δ_1 state cannot find equivalent symmetry in the opposite electrode with reversed magnetization. The spin asymmetry is predicted to increase above 1000%. On the other hand, when the thickness of the insulating layer decreases, the contribution of the double degenerate pd character state Δ_5 and even $\Delta_{2,2'}$ becomes significant, the conduc-

* Corresponding author.

0921-5107/$ – see front matter © 2005 Elsevier B.V. All rights reserved.
doi:10.1016/j.mseb.2005.09.054

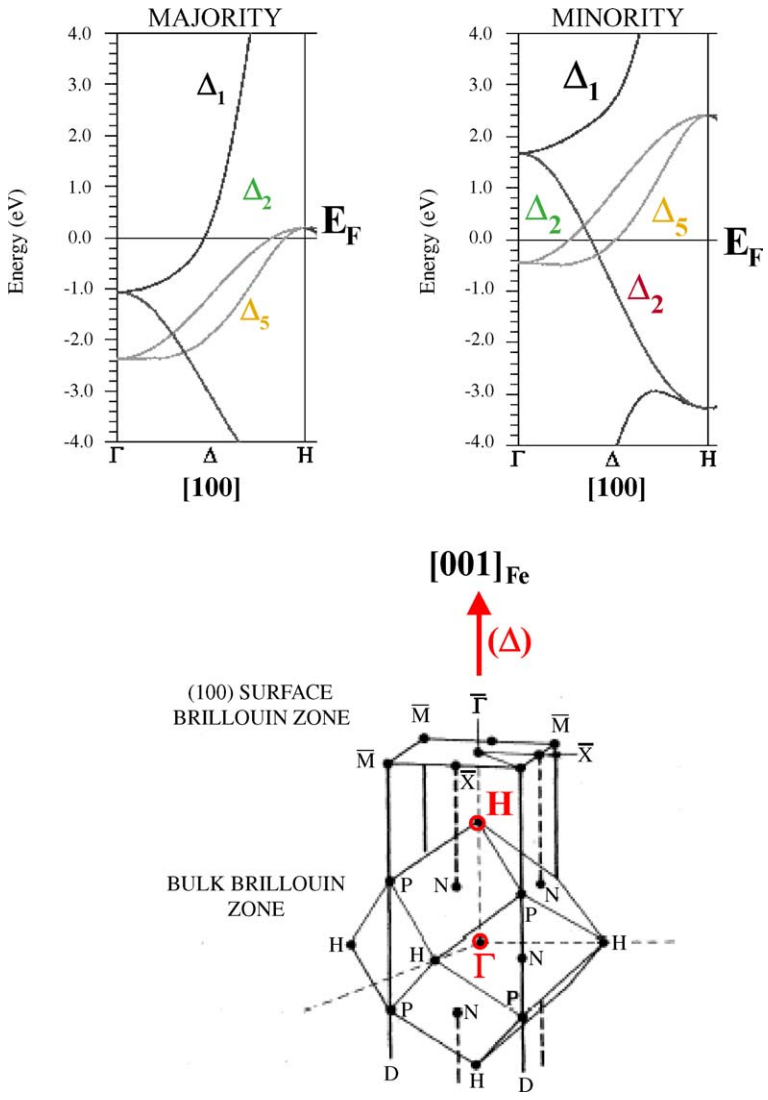

Fig. 1. Top: Bulk energy bands for the majority and minority spins in bcc Fe. Bottom: Representation of the bulk and the (0 0 1) surface Brillouin zone for the bcc Fe.

tivity in the AP state increases and therefore the TMR ratio decreases.

In the thin MgO barrier thickness regime, the tunnel transmission becomes strongly affected by resonant effects at the interfaces [8,6,7,10]. Indeed, for the Fe(0 0 1)/MgO interface, an interfacial minority density of states (DOS) is found above the Fermi energy. The interfacial resonance states from both sides of the barrier may couple to each other leading to a resonant tunneling mechanism [8] which manifests itself as spikes in the conductivity distribution in particular $K_{\parallel}$ points in the two-dimensional Brillouin zone. The width of these spikes is determined by the strength of the coupling in the barrier, which decreases exponentially with the barrier thickness. Consequently, the conductance from an interfacial resonance state is particularly important for thin barriers. The contribution of the resonant assisted tunneling is major in the equilibrium regime and determines the antiferromagnetic coupling interactions observed in our Fe/MgO/Fe system [11]. Alternatively, the contribution to the tunneling of an interfacial state may be activated by biasing the junction at finite bias voltage, even at large MgO thickness regime.

2. Sample elaboration

The MTJ multilayer stacks subjected to our studies have been elaborated by molecular beam epitaxy (MBE), in a chamber with a base pressure of 5×10^{-11} Torr. Two set of samples have been grown on (1 0 0) MgO substrates, previously annealed at 600 °C for 20 min. For the sample type A, a 50 nm thick bottom Fe layer was deposited at room temperature directly on the MgO substrate. For the sample type B, a 10 nm thick seed MgO under-layer was grown at 450 °C on the substrate before the deposition of the 50 nm thick Fe layer. This MgO under-layer acts as an antidiffusion barrier which traps the residual carbon impurities and prevents their diffusion within the layers during subsequent annealing stages. Indeed, to improve its surface quality, the bottom Fe layer was annealed at 450 °C for 20 min. The surface RMS roughness after annealing, estimated from atomic force microscope analysis, was about 0.3 nm. However, the Fe top surfaces post-annealing are not equivalent for sample types A and B, as highlighted in Fig. 2a containing reflecting high energy electron diffraction (RHEED) patterns. For both sets of samples, the

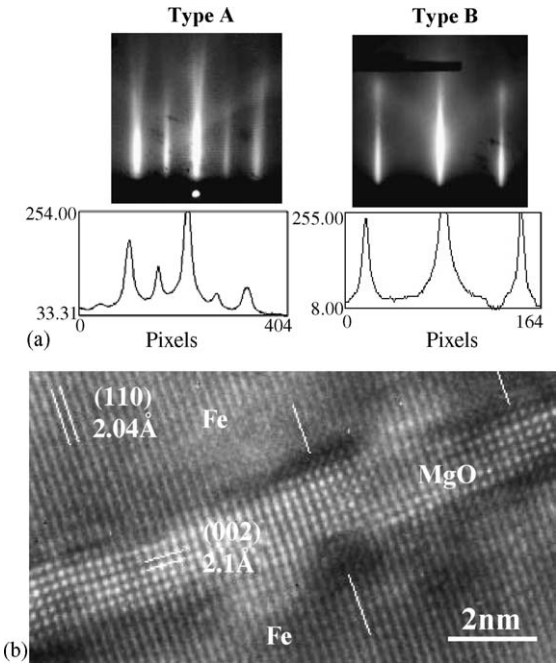

Fig. 2. (a) RHEED patterns measured along the [1 0 0] direction of the Fe bottom layer in sample type A (left) and sample type B (right). The profile analysis for sample A highlights additional peaks characteristic of the 2 × 2 reconstruction. (b) Cross section transmission electron microscopy image of Fe/MgO/Fe stack. TEM analysis performed by E. Snoeck, CEMES Toulouse.

RHEED patterns along the [1 1 0] direction (not shown here) are identical and they are characteristic of the bcc Fe structure. However, along the [1 0 0] direction, the RHEED analysis of sample type A emphasizes a 2 × 2 reconstruction-related additional pattern, not present for sample B. A complete RHEED analysis concludes that in samples type A, the Fe surface post-annealing presents a $c(2 \times 2)$ super-structure. In agreement with results of previous Auger electron spectroscopy and quantitative low-energy electron diffraction (LEED) studies [12], we associate this reconstruction to the segregation of C at the Fe(0 0 1) surface. Using Auger analysis we checked the chemical nature the surface and we confirmed that for sample type A, a carbon monolayer was segregated during the Fe annealing. Where the C comes from? We observed that the annealing stage of the MgO substrate at 600 °C does not desorbs all the C atoms from the surface. In case when the antidiffusion 10 nm MgO thick underlayer is not inserted (sample type A), the residual C atoms diffuse and segragate to the Fe top surface and provide the surface reconstruction during the bottom Fe layer annealing. On the other hand, in the samples type B, the trapping under-layer of MgO provides a C free Fe top surface, post-annealing. As it will be shown in the following, the chemical structure of the Fe surface has a strong impact on the magneto-transport characteristics of the junctions mainly reflected by the TMR versus applied voltage behaviour.

On the top of the bottom Fe layer, the MgO insulating layer was epitaxialy grown by means of an electron gun. A two-dimensional layer-by-layer growth was observed up to five monolayers by means of RHEED intensity oscillations [13]. These oscilations have been used to control precisely the thickness of the barrier in the extremely thin thickness range from three to six monolayers, used for magnetic coupling studies. For the systems used to study the magneto-transport properties, the thickness of the insulating barrier was fixed to 3.0 nm. This thickness corresponds to the asymptotic regime where we expect as predicted theoretically large magnetoresistive effects. A second magnetic 10 nm thick Fe layer was epitaxially grown on the top of the insulating MgO barrier at 100 °C. It was subsequently annealed for flattening at 380 °C for 10 min for samples type B whereas for samples type A this annealing stage was not performed in order to avoid possible structural modification of the bottom Fe–C/MgO interface. This top Fe layer is magnetically hardened by a 20 nm Co under-layer. The stack was capped with a Pd(10 nm)/Au(10 nm) protecting bilayer.

The structural quality of the tunnel junction stack is illustrated by the cross-section transmission electron microscopy picture, depicted in Fig. 2b. One can see the epitaxial growth of MgO on Fe. This is a key parameter for the conservation of symmetry from the Fe electrode through the MgO barrier (conservation of $K\|$) and has a huge impact on the Bloch wave propagation in the stack. However, dislocations located either at the bottom or at the top Fe/MgO interface (indicated in the picture by dark zones pointed by white lines) induce a violation of symmetry conservation and therefore have detrimental effects in the symmetry filtering.

After the MBE growth of the multilayer stack, the MTJ structures are patterned by UV lithography and Ar ion etching, step-by-step controlled in situ by Auger spectroscopy [13].

3. Spin polarized tunnel transport in Fe/MgO/Fe junctions

3.1. Equilibrium tunnel transport-coupling regime

In the very thin MgO thickness regime (three to five monolayers), we observe antiferromagnetic (AF) coupling interactions at room temperature between the two ferromagnetic (F) Fe layers separated by the thin insulating tunnel barrier. We associate these interactions to the transport of spin information across the insulating spacer by equilibrium quantum tunneling of spin polarized electrons [11]. Equilibrium tunneling implicates tunneling of majority and minority electrons from one side to the other of the junction. In the absence of any net bias, the total current across the insulating MgO barrier is zero.

The magnetic properties have been investigated from magnetization versus field loops performed on continuous multilayer films with lateral sizes above a few millimeters in order to avoid spurious antiferromagnetic dipolar coupling, introduced by patterning of small size devices. The interlayer magnetic coupling strength J is extracted from the shift of the minor hysteresis loops (inset of Fig. 3) taken for the soft magnetic layer in a field window where the hard layer is magnetically 'locked' by an initial magnetization saturation. In Fig. 3, we illustrate the variation of J with the thickness t_{MgO} of the insulating barrier. The AF coupling interactions have been observed for both type of samples A and B, with and without carbon at the Fe/MgO interface.

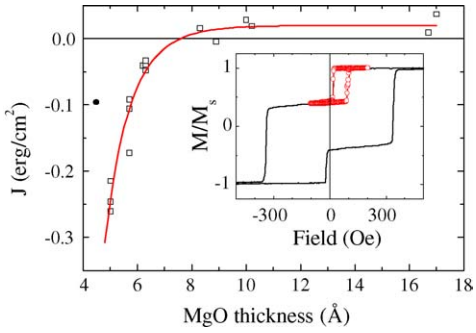

Fig. 3. Variation of the coupling strength with the MgO thickness. The open square points represent experimental values and the continuous line a theoretical calculations within the Slonczewski model of coupling by spin-polarized tunneling. Inset: magnetization vs. field curve and minor loop (◯). From the positive shift of the minor loop H_{ex} one can extract the coupling strength $J : H_{ex} = J/(t_{Fe}M_s)$, where t_{Fe} is the thickness of the Fe bottom layer and M_s the saturation magnetization of Fe.

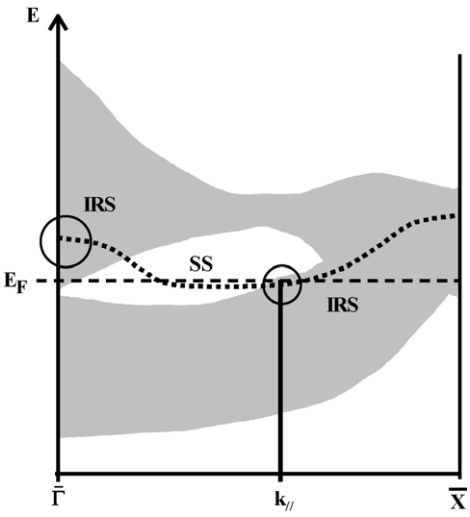

Fig. 4. Simplified diagram for the dispersion of the surface energy bands for minority spin in Fe(0 0 1) as reported by Stroscio et al. [17]. The grey zones represent (schematic) the bulk bands, whereas the dash line the dispersion of the surface state (SS). When the surface state lies within a bulk band, it becomes interfacial resonance state (IRS), and can contribute to the transport towards the bulk, i.e. in $\bar{\Gamma}$ point above E_F and for a certain value $k\| \neq 0$ at E_F.

One can see the experimental points and also the continuous line which represents the theoretical coupling strength computed in the simplified free-electron-like framework of Slonczewski, as explained in detail in our previous paper [11]. The theoretical curve implicates effective parameters for the electronic transport, specific to the ferromagnetic Fe electrodes and the MgO insulator. However, the model of Slonczewski does not take into account the specific aspects of the spin polarized tunneling in epitaxial systems i.e. the equilibrium propagation of different symmetry states for each spin channel, in each configuration of magnetization: (i) in the parallel (P) configuration the $\Delta_{1,5,2'}$ states for the majority spin and $\Delta_{5,2,2'}$ states for the minority; (ii) in the AP configuration $\Delta_{5,2'}$ states for the majority and for the minority spin. Moreover, the equilibrium tunnel transport in the AP configuration is dominated by the propagation of the interfacial resonance of Fe(0 0 1) having a d_{z^2} orbital character, located in the minority channel [6,7]. The conductivity presents extremely sharp peaks located at specific values of $k\|$. Interestingly, these peaks does not correspond, as typically expected within the free-electron model to electrons, to a k normal to the insulator ($k\| = 0$). One can show that the peaks in the conductivity are directly related to the minority spin surface state of Fe(0 0 1) represented in the sketched diagram of the minority surface band structure of Fe(0 0 1) shown in Fig. 4. At the Fermi level, the surface state crosses E_F for a specific value $k\|$. Moreover, the contribution to the conduction of the surface state becomes significant when it lies within a bulk band (dark areas in the E–k diagram), situation when the surface state becomes interfacial resonance state (IRS). The implication of a resonance assisted tunneling mechanism in the AF coupling by spin polarized tunneling has been theoretically mentioned by Tsymbal et al. [14]. In their model, they have shown that an additional resonant tunneling mechanism should exist in order to explain the sign of the coupling observed in our Fe/MgO/Fe junctions. If we neglect any impurity-associated resonant levels, the interfacial minority resonance of Fe provides the resonant equilibrium tunneling mechanism as also shown in the ab-initio calculations of Dederichs et al. [8]. Therefore, the propagation of the interfacial resonance could be the main responsible for the AF coupling observed in our Fe/MgO/Fe junctions.

The physics of the equilibrium tunneling presented above seems pretty complex due to the implication in the coupling of different symmetry states and also of the interfacial resonance of Fe. This would implicate a multi-channel tunneling model, each tunneling channel being associated to a specific symmetry-related or resonance state. However, the conciliation with the simplified mono-channel model of Slonczewski may be done if we consider that the parameters used within this model are effective, and include the complex aspects of multi-channel tunneling landscape, mentioned upwards.

3.2. Non-equilibrium tunnel transport

The tunneling phenomena get different in the asymptotic regime at large MgO thickness where the symmetry-dependent rate decay in the barrier will reduce the number of propagating states. However, we should mention that in this regime, the structural quality of the MgO layer is slightly reduced. Indeed, after a pseudomorphical growth of MgO on Fe up to about five monolayers, a plastic relaxation occurs. This will induce dislocations within the barrier. These dislocations behave as local ‘defects’ where the symmetry is broken. Therefore, they induce additional scattering with detrimental effects in the symmetry filtering.

The analysis of this regime is performed using magneto-transport measurements (non-equilibrium regime) on patterned tunnel junctions with lateral size between 50 and 200 μm.

Lets us first consider the TMR(V) characteristics illustrated in Fig. 5a measured on sample B with carbon free Fe/MgO interface. As predicted theoretically [6,7], for large MgO thickness in the asymptotic regime, the tunneling is found to be dominated by a majority spd-like character state Δ_1 in the parallel

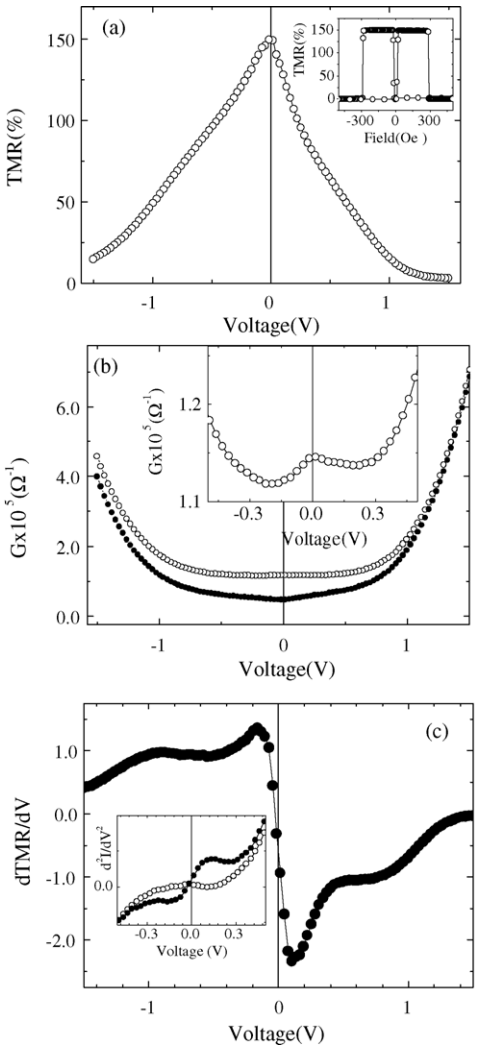

Fig. 5. Magnetotransport characteristics for sample type B in *P* configuration (◯) and AP configuration (●). In positive bias, the current flows from the top to the bottom electrode of the MTJ. (a) Bias variation of the TMR. Inset: Typical TMR vs. field loop measured at 10 mV. (b) Conductivity ($G = I/V$) vs. voltage curve, in the parallel respectively antiparallel configuration of magnetization. Inset: Zoom around zero voltage illustrating local minima in the *P* conductivity. (c) First derivative of the TMR vs. voltage. Inset: d^2I/dV^2 spectra, at low voltage. One can remark positive peaks in the AP configuration.

(*P*) configuration. The propagation of this state in the antiparallel (AP) configuration should be prohibited, which corresponds to a strongly reduced conductivity. Within this framework, we measure a large TMR signal, above 150% at room temperature. The slightly asymmetric bias-dependence can be explained by asymmetric top and bottom Fe/MgO interfaces in terms of roughness, structural defects (dislocations) and the lattice distortions. The limited maximum value of the TMR with respect to theoretical predictions implicates a loss in the filtering efficiency due to the structural imperfections enumerated above over the large area junctions. We mention that all the junctions subjected to our study have a lateral size larger than 50 μm, which is 500 times larger than the submicronic junctions in which higher TMR effects have been reported by other groups [4,5]. Moreover, the TMR shows a strong variation with the applied voltage, especially in the small voltage range. From the conductivity in the *P* and AP configuration (depicted in Fig. 5b), we see that basically, the decrease of the TMR is mainly related to the increase of the AP conductivity with the bias voltage. The conductivity in the parallel configuration presents a local minimum around 0.2 eV, in both positive and negative voltage (see inset in Fig. 5b). This minimum reflects the dispersion of the energy bands of Fe(0 0 1), see Fig. 1. The top of the Δ_5 band lies at about 0.2 eV above the Fermi level. When the energy of the hot electrons arriving across the barrier overcomes the top of this Δ_5 band, the conduction channel associated to this symmetry disappears. Therefore, the minimum of the *P* conductivity validates a Δ_5 contribution to the tunneling at small bias (imperfect filtering).

The increase with the bias voltage of the AP conductance can be understood from tunneling spectroscopy analysis. If we analyze the derivative of the TMR as a function of the voltage (shown in Fig. 5c) and second derivative of the current (inset of Fig. 5b) we can see peaks similar to those located at the 'inelastic' excitation energy [15] in standard tunnel junctions. In our junctions we associate these peaks to resonant tunneling transport. Indeed, if we neglect the spin-flip phenomena, the expected AP conductivity is small: in the AP configuration an injected Δ_1 state cannot find an equivalent symmetry in the second electrode. Any spin-flip mechanism could drive a majority up Δ_1 state into a majority down Δ_1 state in the second electrode and increase drastically the conductivity. However, we do not need to evoke spin-flip mechanisms if we consider the electronic structure of the Fe(0 0 1) interface. If one takes into account the minority interfacial resonance of Fe having a d_z^2 orbital character and belonging to a Δ_1 symmetry, one can see that when this resonance gets activated (see Fig. 4), the AP conductivity will be strongly enhanced (an injected Δ_1 state will find an available state with similar symmetry in the opposite electrode with reversed magnetization, via the interfacial resonance [9].

On the other hand, the TMR(V) characteristic measured on sample A, with carbon impurities at the bottom Fe/MgO interface, appears strongly asymmetric with a maximum of TMR of 126% at room temperature (see Fig. 6a). This asymmetry reflects a net signature of the bcc Fe(0 0 1) electronic structure, mainly the contribution to the tunneling of the interfacial resonance of Fe having a d_{z^2} orbital character. The signature of the interfacial resonance in the tunneling has already been shown for systems with smaller MgO thickness [16]. Here, as expected for the rapid decay of the d-like states in the MgO barrier, the conductivity associated to this interfacial resonance should be overwhelmed at 3 nm thickness of MgO, by the dominance of the Δ_1 conduction channel. The vanishing of the surface resonance contribution to the tunneling in the asymptotic regime has already been reported by Ding et al. [10]. In our systems, this is what happens in sample type B, with clean Fe/MgO interfaces. However, when carbon impurities are inserted at the Fe/MgO bottom interface, the bonding between C and Fe (mainly via s,p-like orbitals) will drastically affect the propagation of the Δ_1 symmetry without affecting the interfacial resonance of Fe located in a d-like orbital. Preliminary ab-initio calculations [18] of Fe–C/MgO electronic structure show that the only effect of C

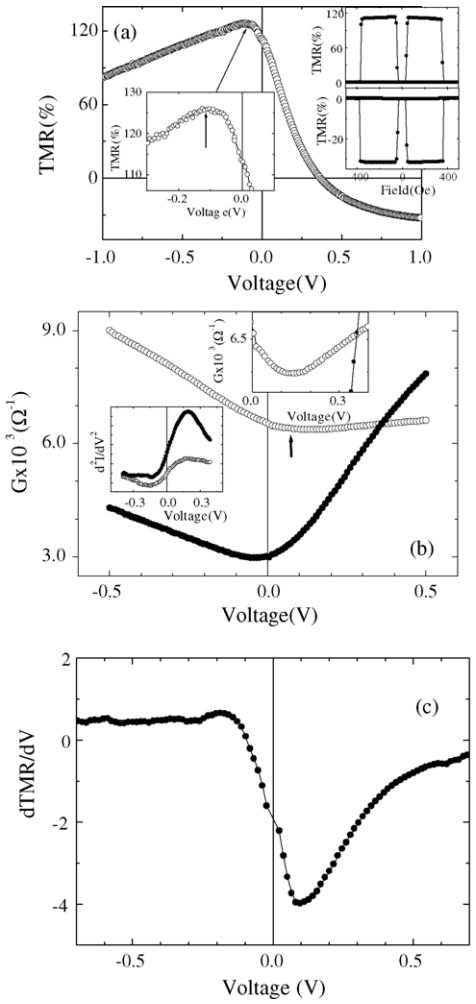

Fig. 6. Magnetotransport characteristics for sample type A in *P* configuration (◯) and AP configuration (•). In positive bias, the current flows from the top to the bottom electrode of the MTJ. (a) Bias variation of the TMR. Right inset: Typical positive TMR–H loop measured at −10 mV, and negative TMR–H curve measured at +0.6 V, after the TMR reversal. Left inset: Zoom around the maximum of the TMR. (b) Conductivity ($G = I/V$) vs. voltage curve, in the parallel and antiparallel configuration of magnetization. Top inset: Zoom around the local minima of the parallel conductivity. Bottom inset: d^2I/dV^2 spectra, at low voltage. One can remark positive peaks in both *P* and AP configuration. (c) First derivative of the TMR vs. voltage.

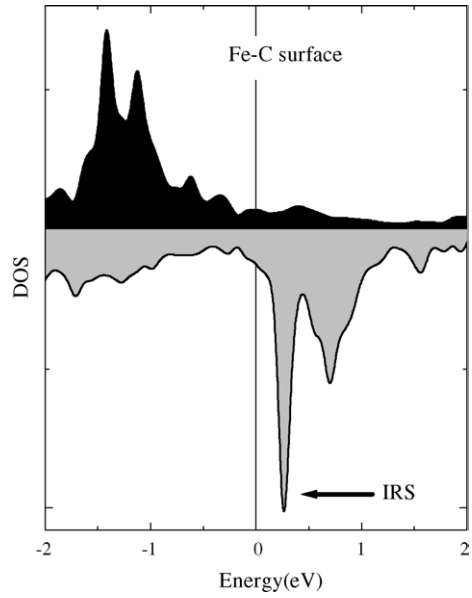

Fig. 7. Surface density of state for majority (black) and minority (gray) spins, in an energy range ±2 eV around the Fermi level, for the interfacial Fe contaminated by C impurities, in a Fe/Fe–C/MgO stack. The calculation was performed using full potential linear augmented plane wave method [19]. One can remark the minority IRS of Fe–C surface, at ∼0.3 eV above the E_F.

at the interface on the surface state of Fe is a slight shift upwards in energy, with respect to the carbon free interface (Fig. 7). Similar effects, concerning the localization of Δ_1 electrons in the interfacial bonding have been reported by Zhang et al. for oxygen impurities located at the interface Fe/MgO [20]. Moreover, as long as the conductivity of the s-like character state of the Δ_1 channel is reduced, one can expect a significant contribution to the tunneling of the Δ_5 with a pd character. Therefore, the TMR(V) will reflect the spectroscopy of the density of d-like states of the bcc Fe(0 0 1).

For positive biasing of the bottom electrode, the electrons extracted from the top Fe(0 0 1) electrode by tunneling across the barrier, 'scan' in energy the bottom 'flat' Fe(0 0 1) electronic structure. Then, when the energy of the collected electrons 'matches' the energy of the interface resonant state, a strong enhancement of the antiparallel conductivity with respect to the parallel one occurs, via the enhancement of the wave function matching at the interface. This is directly reflected by the sign reversal of the TMR (inset of Fig. 6a) and by the antiparallel conductance which overcomes the parallel one above 0.2 eV, see Fig. 6b. Here again, the *P* conductivity presents a minimum, when the energy of the hot electrons overcomes the one of the Δ_5 band. The voltage variation features can be easily analyzed using the derivative of the TMR with respect to the external bias illustrated in Fig. 6c. The strong dip in the derivative in the positive bias corresponds to the activation of the resonant assisted tunnel mechanism by the minority IRS, above 0.2 eV when it gets in $k\| = 0$ (as shown in the sketch of Fig. 4).

The structural quality of the top MgO/Fe interface is reduced with respect to the atomically flat bottom one. Indeed, the bottom Fe was annealed at 450° whereas the top Fe electrode in junction type A was not. The RHEED patterns and also the Atomic Force Microscopy experiments validate a significantly higher roughness of the top Fe electrode in sample type A. One can assume that the interfacial resonance is destroyed by roughness for this electrode, and also that the density of states of the rough electrode presents no sharp features.

For negative voltage, when the electrons tunnel towards the rough top electrode positively biased, we observe a very small variation of the magnetoresistance versus V ($V_{1/2} > 1.5V$) (also illustrated by $dTMR/dV$ see Fig. 6c). Moreover, the maximum of the TMR is not centered in zero bias, which implicates an increase of the TMR with the voltage (left inset in Fig. 6a). The increase of the TMR with the applied bias has been already theoretically predicted by Zhang et al. [21]. The increase originates from an increase of the tunneling polarization/filtering efficiency of the emitter bottom electrode due to the contribu-

tion to the tunneling of the electrons from the bottom negatively biased electrode located below the Fermi level within an energy range $[E_F - eV, E_F]$. This contribution is dominated by the decrease of the minority IRS contribution to the conductivity (non negligible at zero bias) respectively activation of contribution of majority IRS located below E_F [21]. Moreover, the extremely small decay of the TMR with the negative applied voltage implicates that a electronic-structure voltage variation mechanism related to the bottom Fe electronic structure competes with all the mechanisms responsible for the zero bias anomaly, observed in sample type B, where a significant decay of the TMR with bias has been measured.

These mechanisms are: (i) incoherent tunneling due to scattering at impurities or defects located in the barrier [22]; (ii) energy dependence of spin polarized DOS which affects the spin polarization [23]; (iii) quenching of TMR by hot electrons or spin excitation of magnons [24]. In our monocristalline MTJ, the first mechanism should not be dominant. Here, the quality of the insulator is rigorously controlled by the 2D epitaxial growth. However, one cannot exclude the dislocations within the insulating barrier, after the plastic relaxation. This will induce imperfect filtering effects. Concerning the second mechanism, one can assume that the energy dependence of spin polarized DOS of a rough electrode, above the Fermi level is small (no sharp features). Therefore, the electronic structure contribution to the TMR(V) is mainly related to the electronic structure below E_F of the bottom flat Fe electrode. This contribution should compete with the inelastic tunneling mechanisms responsible on the TMR(V) decay observed in samples type B. In sample type B, where the tunneling of s-like Δ_1 electrons is dominant, the contribution of the d-DOS features to the TMR(V) is expected to be 'negligible'. Here, the DOS mechanism which should compete to the decay of the TMR (as seen in samples type A) is not 'activated'.

The completely different voltage behaviour of junction types A and B shows the major importance of carbon impurities at the bottom interface. The role of these impurities is to select the tunneling electrons in terms of their orbital character. By reducing the conductivity of the Δ_1 electrons in carbon contaminated junctions the tunnel transport gets sensitive to the d-like features, which otherwise were attenuated at large MgO thickness. Our results show that the interface engineering in Fe/MgO/Fe MTJs represents a strong tool to control the magneto-transport properties of spintronic devices.

In the thin MgO thickness regime, the carbon impurities at the Fe/MgO interface play no significant role in the tunneling. Indeed, no significant effect of the C on the antiferromagnetic interactions has been observed. If we consider the complex tunneling landscape in this regime, one can see that the ' bonding does not affect the d_{z^2}-like resonance state of Fe, whose propagation dominates the equilibrium tunneling currents.

4. Conclusion

Spin polarized transport properties in epitaxial Fe/MgO/Fe single crystal tunnel junction stacks have been investigated in two 'extreme' regimes. First, for very thin MgO layers, we show that the equilibrium tunnel transport between the two Fe electrodes across the barrier induces an interesting antiferromagnetic interaction. This antiferromagnetic coupling effect is explained in terms of spin-polarized tunneling. If we take into account the specific aspects of the electronic transport in monocrystalline multilayers, one has to consider a complex, symmetry-related multi-channel model for the tunneling with a dominant contribution of the Fe(0 0 1) minority spin resonance state, whose dominant tunneling determines the sign of the coupling. Second, for large MgO thickness in the asymptotic regime, we observed as predicted theoretically, large magnetoresistive effects, directly related to the band structure characteristics of the Fe/MgO/Fe junctions. Moreover, we illustrate that the interface chemical structure plays a crucial role in the filtering of tunneling electrons in terms of symmetry and orbital character. Therefore, the magneto-transport properties of epitaxial tunnel junctions may be skillfully engineered to achieve new functionality when the tunnel junction is used as an elementary brick in any spintronic devices.

Acknowledgment

The authors are grateful to D. Stoeffler for stimulating discussions.

References

[1] J.S. Moodera, L.R. Kinder, T.M. Wong, R. Meservey, Phys. Rev. Lett. 74 (1995) 3273.
[2] S.A. Wolf, J. Supercond. 13 (2000) 195;
J.M. Daughton, J. Appl. Phys. 81 (1997) 3758;
W.J. Gallagher, J.H. Kaufman, S.S.P. Parkin, R.E. Scheuerlin, U.S. Patent No. 5,640,343 (1997).
[3] S. Yuasa, T. Nagahama, A. Fukushima, Y. Suzuki, K. Ando, Nat. Mater. 3 (2004) 868.
[4] S.S.P. Parkin, C. Kaiser, A. Panchula, P.M. Rice, B. Hughes, M. Samant, S.-H. Yang, Nat. Mater. 3 (2004) 862.
[5] D.D. Djayaprawira, K. Tsunekawa, M. Nagai, H. Maehara, S. Yamagata, N. Watanabe, S. Yuasa, Y. Suzuki, K. Ando, Appl. Phys. Lett. 86 (2005) 092502.
[6] J.M. MacLaren, X.-G. Zhang, W.H. Buttler, X. Wang, Phys. Rev. B 59 (1999) 5470;
W.H. Butler, X.-G. Zhang, T.C. Schulthess, J.M. MacLaren, Phys. Rev. B 63 (2001) 054416.
[7] J. Mathon, A. Umerski, Phys. Rev. B 63 (2001) 220403R.
[8] O. Wunnicke, N. Papanikolaou, R. Zeller, P.H. Dederichs, V. Drchal, J. Kudrnovsky, Phys. Rev. B 65 (2002) 064425.
[9] C. Tiusan, et al., Phys. Rev. B, submitted for publication.
[10] H.F. Ding, W. Wulfhekel, J. Henk, P. Bruno, J. Kirchner, Phys. Rev. Lett. 90 (2003) 116603.
[11] J. Faure-Vincent, C. Tiusan, C. Bellouard, E. Popova, M. Hehn, F. Montaigne, A. Schuhl, Phys. Rev. Lett. 89 (2002) 107206.
[12] V. Blum, A. Schmidt, W. Meier, L. Hammer, K. Heinz, J. Phys.: Condens. Matter 15 (2003) 3517.
[13] E. Popova, J. Faure-Vincent, C. Tiusan, C. Bellouard, H. Fischer, M. Hehn, F. Montaigne, M. Alnot, S. Andrieu, A. Schuhl, E. Snoeck, V. da Costa, Appl. Phys. Lett. 81 (2002) 1035;
J. Faure-Vincent, C. Tiusan, E. Jouguelet, F. Canet, M. Sajieddine, C. Bellouard, E. Popova, M. Hehn, F. Montaigne, A. Schuhl, Appl. Phys. Lett. 82 (2003) 4507.
[14] M.Ye. Zhuravlev, E.Y. Tsymbal, A.V. Vedyayev, Phys. Rev. Lett. 94 (2005) 026806.

[15] J.S. Moodera, J. Nowak, R.J.M. Veerdonk, Phys. Rev. Lett. 80 (1998) 2941.
[16] C. Tiusan, J. Faure-Vincent, C. Bellouard, M. Hehn, E. Jouguelet, A. Schuhl, Phys. Rev. Lett. 93 (2004) 106602.
[17] J.A. Stroscio, D.T. Pierce, A. Davies, R.J. Celotta, Phys. Rev. Lett. 75 (1995) 2960.
[18] We calculated the electronic structure of the Fe/Fe–C/MgO/Fe stack using the full potential-linear augmented plane wave (FP-LAPW) Wien2k code [19]. In our calculation, we used a supercell consisting of 10 Fe layers, sandwiched in-between six MgO layers. In order to describe the Fe–C/MgO interface a monolayer of C has been alternatively considered at 0.4 Å above the interfacial Fe.
[19] P. Blaha, K. Schwarz, G.K.H. Madsen, D. Kvasnicka, J. Luitz, WIEN2k: An Augmented Plane Wave + Local Orbitals Program for Calculating Crystal Properties, K. Schwartz, Techn. Univ., Wien, Austria, 2001, 3-9501031-1-2.
[20] X.-G. Zhang, W.H. Butler, A. Bandyopadhyay, Phys. Rev. B 68 (2003) 092402.
[21] C. Zhang, X.-G. Zhang, P.S. Krstic, H.-P. Cheng, W.H. Butler, J.M. MacLaren, Phys. Rev. B 69 (2004) 134406.
[22] R. Jansen, J.S. Moodera, Phys. Rev. B 61 (2000) 9047.
[23] J.M. de Teresa, A. Barthelemy, A. Fert, J.P. Contour, F. Montaigne, P. Seneor, Science 286 (1999) 507.
[24] S. Zhang, P.M. Levy, A.C. Marley, S.S.P. Parkin, Phys. Rev. Lett. 79 (1997) 3744;
J.S. Moodera, J. Nowak, R.J.M. van de Veerdonk, Phys. Rev. Lett. 80 (1998) 2941.